MRS Advances © 2018 Materials Research Society
DOI: 10.1557/adv.2018.40

Fabrication of silicon nanowire based solar cells using TiO_2/Al_2O_3 stack thin films

Yasuyoshi Kurokawa[1,2], Ryota Nezasa[1], Shinya Kato[3], Hisashi Miyazaki[4], Isao Takahashi[1], Noritaka Usami[1]

[1]*Graduate School of Engineering, Nagoya University, Furo-cho, Chikusa-ku, Nagoya, Aichi, 464-8603, Japan*
[2]*PRESTO, Japan Science and Technology Agency (JST), 4-1-8 Hon-cho, Kawaguchi-shi, Saitama, 332-0012, Japan*
[3]*Department of Frontier Materials, Nagoya Institute of Technology, Gokiso-cho, Showa-ku, Nagoya, Aichi, 466-8555, Japan*
[4]*Department of Materials Science and Engineering, National Defense Academy, 1-10-20 Hashirimizu, Yokosuka-shi, Kanagawa 239-8686, Japan*

ABSTRACT

To improve conversion efficiency of silicon nanowire (SiNW) solar cells, it is very important to reduce the surface recombination rate on the surface of SiNWs, since SiNWs have a large surface area. We tried to cover SiNWs with aluminum oxide (Al_2O_3) and titanium oxide (TiO_2) by atomic layer deposition (ALD), since Al_2O_3 grown by ALD provides an excellent level of surface passivation on silicon wafers and TiO_2 has a higher refractive index than Al_2O_3, leading to the reduction of surface reflectance. The effective minority carrier lifetime in SiNW arrays embedded in a TiO_2/Al_2O_3 stack layer of 94 μsec was obtained, which was comparable to an Al_2O_3 single layer. The surface reflectance of SiNW solar cells was drastically decreased below around 5% in all of the wavelength range using the $Al_2O_3/TiO_2/Al_2O_3$ stack layer. Heterojunction SiNW solar cells with the structure of ITO/p-type hydrogenated amorphous silicon (a-Si:H)/n-type SiNWs embedded in Al_2O_3 and TiO_2 stack layer for passivation/n-type a-Si:H/back electrode was fabricated, and a typical rectifying property and open-circuit voltage of 356 mV were successfully obtained.

INTRODUCTION

Silicon nanowires (SiNWs) have recently attracted much attention as one of the novel photovoltaic materials. It is expected that SiNW solar cells [1-13] with a relatively thin absorber layer will have the potential to realize sufficient photocurrent [14-22]. It is very important to reduce the surface recombination rate on the surface of SiNWs, since SiNWs have a large surface area. We confirmed the high passivation effect of Al_2O_3 deposited by atomic layer deposition (ALD) on SiNW arrays by measuring the effective minority carrier lifetime [23,24]. Moreover, we fabricated heterojunction SiNW (HJ-SiNW) solar cell structure, and confirmed the solar cell performance [25]. To obtain SiNW solar cells with higher efficiency, it is needed to reduce internal reflection in SiNW solar cells. The previous structure of SiNW solar cells and the reflectance of the fabricated SiNW solar cell are shown in Figs. 1(a, b), respectively [26]. The high

reflectance in the infrared region is due to large refractive index mismatch between the p-type a-Si:H and the n-type SiNWs embedded in Al_2O_3, since the refractive index of the SiNW layer was determined by effective medium approximation (EMA) of crystalline silicon and Al_2O_3 with a low refractive index of 1.6. In this study, to decrease surface recombination, we tried to cover SiNWs with aluminum oxide (Al_2O_3) and titanium oxide (TiO_2) by atomic layer deposition (ALD), since Al_2O_3 grown by ALD provides an excellent level of surface passivation on silicon wafers and TiO_2 has higher refractive index than Al_2O_3, leading to the reduction of surface reflectance. In addition, optical properties and effective carrier lifetime of the SiNWs with the TiO_2/Al_2O_3 stack layer were evaluated.

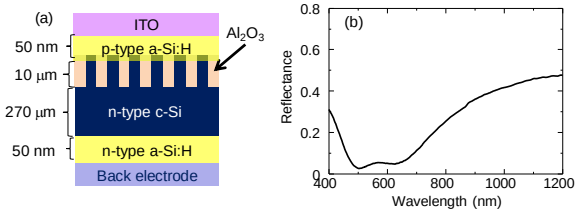

Figure 1. (a) Schematic diagram of previously reported heterojunction SiNW solar cells [26], (b) Reflectance spectrum of the SiNW solar cell.

EXPERIMENTAL DETAILS

SiNW arrays were prepared by metal assisted chemical etching with silica nanoparticles (MACES) [27] on a Si wafer (n-type, (100), 1-5 Ω·cm). Although it is basically the same as the MACE process [28], silica nanoparticles are used as an etching mask to control the diameter and density of SiNWs. After the etching of the native oxide on a Si wafer, the Si wafer was immersed in ethylenediamine ($C_2H_8N_2$) under a nitrogen atmosphere for 3 hours at room temperature. The wafer was rinsed with deionized (DI) water. The hydrophilic Si wafers were immersed in a solution in which 30-nm-silica nanoparticles modified by carboxyl groups were dispersed at 2 ^oC for 1 hour. This process formed a dispersed silica nanoparticle layer on the Si wafer. Subsequently a 20-nm-thick silver film was deposited on the wafers with silica nanoparticles using a DC sputtering system. After that, the wafer was chemically etched by using 4.8M HF and 0.15M H_2O_2 at room temperature to form SiNW arrays. SiNWs with the length of 1, 5, and 10 μm were prepared on a Si wafer by changing etching duration. The wafers were put in a HNO_3 solution to remove silver particles. Finally, the oxide layer existing on the surface of the SiNW array was removed with a HF solution. After the fabrication of SiNW arrays, Al_2O_3 and TiO_2 were deposited by an ALD system (Arradiance, GEMSTAR6). Trimethylaluminum ($Al(CH_3)_3$ (TMA)), tetrakisdimethylaminotitanium ($Ti[N(CH_3)_2]_4$), called TDMAT, and H_2O were used as aluminum, titanium, and oxygen reactant sources, respectively. The TDMAT precursor was heated at 60 ^oC. The thicknesses of Al_2O_3 and TiO_2 were both 20 nm. The other experimental conditions are shown in Table I. After the deposition, post-annealing was carried out at 400 ^oC to increase negative charge density in the Al_2O_3 and TiO_2.

The structure of SiNW arrays was characterized by field emission scanning electron microscopy (FE-SEM) and energy dispersive x-ray spectroscopy (EDS) using JEOL JSM-7001F. The minority carrier lifetime was measured by the μ-PCD method using KOBELCO LTE-1510EP. The excited wavelength and intensity of incident light

were 904 nm and 1 $\times 10^{14}$ cm^{-2}, respectively. The microwave frequency was 9.6 GHz. Optical properties of the SiNWs were measured by an UV-VIS-NIR spectrophotometer (JASCO V-570) and gas-microphone photoacoustic spectroscopy system. The PAS experimental apparatus consists of a 300 W halogen lamp coupled with a monochrometer (Jovin-Yvon H20-IR). The photoacoustic (PA) signal was detected by a microphone and a lock-in amplifier (NF Circuit System 5610B) with a mechanical chopper set at a frequency of about 20 Hz. The wavelength of the excitation light was scanned from 400 to 1600 nm at 5 nm intervals. PA signal intensity was normalized by the signal from a fixed quantity of carbon black to eliminate the effects of the wavelength dependence of the optical apparatus.

A solar cell structure using SiNW arrays covered with TiO_2/Al_2O_3 stack layers was fabricated as shown in Fig. 2. SiNW arrays with a length of 10 μm were prepared by MACES on a Si substrate. After the fabrication of SiNW arrays, 30-nm-thick Al_2O_3/100-nm-thick TiO_2/470-nm-thick Al_2O_3 stack layers were deposited on the surface of SiNW arrays by ALD. After the ALD, SiNW arrays were dipped in 1% HF or were etched by reactive ion etching (RIE) with a CF_4/O_2 mixture gas to remove the passivation layer on only the top of SiNWs. A p-type hydrogenated amorphous silicon (a-Si:H) layer and an n-type a-Si:H layer were prepared by plasma-enhanced chemical vapor deposition (PECVD) on the front and back, respectively. Indium tin oxide (ITO) was deposited on the p-type a-Si:H layer by RF sputtering. Finally, an Al electrode was evaporated on the back of SiNW solar cells. The final structure was ITO/p-type a-Si:H/n-type SiNW arrays embedded in TiO_2 and Al_2O_3/n-type a-Si:H/Al. The surface reflectance of the SiNW solar cells was evaluated by UV-VIS-NIR spectrophotometers with SHIMADZU Solid Spec-3700. The solar cells were characterized by dark and illuminated *J-V* characteristics under AM1.5G illumination.

Table I. Deposition conditions of Al_2O_3 and TiO_2.

Materials	Al_2O_3	TiO_2
Temperature	200 °C	225 °C
Cycles	350	144
Flow duration	TMA: 200 msec	TDMAT: 700 msec
	H_2O: 200 msec	H_2O: 22 msec

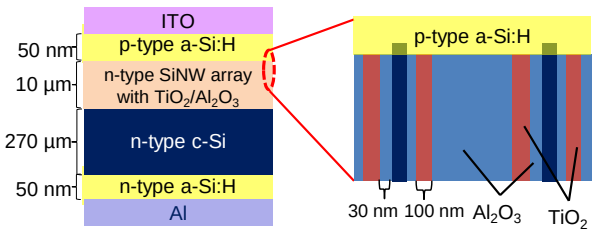

Figure 2. Schematic diagram of the fabricated solar cell structure including SiNW arrays covered with $Al_2O_3/TiO_2/Al_2O_3$ stack layers.

RESULTS AND DISCUSSION

In Figure 3(a), the cross-sectional SEM images of the SiNW array after the deposition of a TiO_2/Al_2O_3 passivation film are shown. From the figure, the length of SiNWs was 15.6 μm. The dark contrast owing to the gap between SiNWs cannot be confirmed, suggesting that the TiO_2/Al_2O_3 stack film perfectly covered SiNWs. Figs. 3(b-e) show the EDS mappings of silicon, aluminum, titanium, and oxygen, respectively. White and black signals show a maximum and minimum value, respectively. Compared with Fig. 3(b) and 3(d), the signal intensity contradicts each other, suggesting that the Al_2O_3 or TiO_2 thin films exist between SiNWs. From a SEM image, the shape of SiNWs around the top is needle-like and the gap between SiNWs is about several hundred nanometers. Therefore, the Al and Ti intensities around the top of SiNWs is stronger than the bottom region. These results also suggest that the TiO_2/Al_2O_3 stack film covered SiNWs from the top to the bottom.

Figure 4 shows external absorption spectra of (a) Al_2O_3, (b) TiO_2, and (c) TiO_2/Al_2O_3 coated SiNW arrays. The thickness of Al_2O_3 and TiO_2 is 20 nm, respectively. In Fig. 4(a), for the flat substrate, the absorptance in the visible light region decreased mostly due to the high reflectance by about 40%. On the other hand, for all of the SiNW arrays, almost 100% absorption was obtained, suggesting that fabricated SiNW arrays have a very high optical confinement effect. The samples coated with TiO_2 have the same trend. When both figures were compared, in the near-infrared region, which is generally a non-absorption region for bulk silicon, the absorptance spectra between (a) Al_2O_3 and (b) TiO_2 are very different. In the case of Al_2O_3-coated-SiNW, there is little absorption above the wavelength of 1200 nm. This is reasonable because bulk silicon and Al_2O_3 do not generally have any absorption in the range except free carrier absorption and absorption related to defects. On the other hand, TiO_2-coated-SiNW has very large absorption. Moreover, the absorption increased with increasing length of the SiNWs. Since the absorption in the region was not detected in the flat substrate after the deposition of TiO_2, it was predicted that absorption sites in the bandgap were generated at the TiO_2/SiNW interface. In the case of the TiO_2/Al_2O_3 stack layer, although the absorption in the infrared region was reduced a little compared to TiO_2-coated SiNW, a high value above 80% was kept. Chen *et al*. have reported that when lattice disorder in hydrogenated anatase TiO_2 nanocrystals was introduced, mid-gap electronic states were created, accompanied by a reduced bandgap [29]. According to this paper, it is possible that the disorder may be introduced into TiO_2 films at the interface between TiO_2/SiNW and the absorption of mid-gap electric states was generated.

Figure 5 shows absorption spectra measured by photoacoustic spectroscopy. Fig. 5 also has the same trend as Fig. 4. The variation of absorption around 1120 nm, which is around the absorption edge of bulk Si, should be noted. In the case of Al_2O_3, the signal was decreased remarkably at the region (Fig. 5(a)). On the other hand, in TiO_2-coated-SiNWs, the variation is very small (Fig. 5(b)). This suggests that TiO_2-coated-SiNWs have a large absorption in wavelengths longer than 1120 nm. Such a high absorption in such a wide range was also observed in the TiO_2/Al_2O_3 stack film shown in Fig. 5(c). On the other hand, the flat Si wafer with the TiO_2/Al_2O_3 stack layer did not have such a high absorption in the same range, suggesting that both SiNW structure and the TiO_2/Al_2O_3 stack layer enhanced the optical confinement. The absorption of an infrared region may be due to the parasitic absorption of disordered TiO_2. Although such a parasitic absorption does not contribute to the photoelectric conversion, it is possible to realize efficient photothermal conversion devices [30].

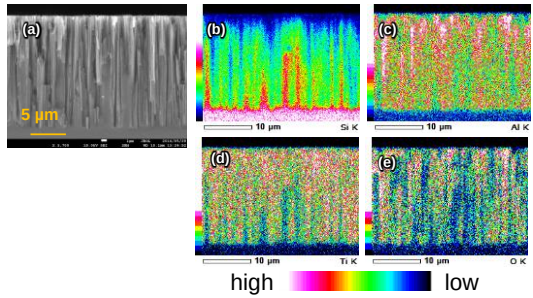

Figure 3. (a) Cross-sectional SEM image and (b-e) EDS mapping of the SiNW array after deposition of TiO_2/Al_2O_3 stack film. (b) Si, (c) Al, (d) Ti, and (e) O.

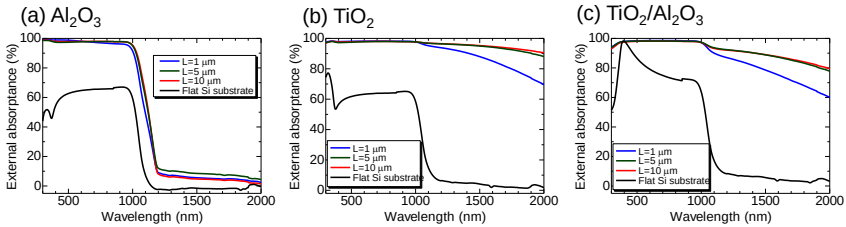

Figure 4. External absorptance calculated from measured transmittance and reflectance. (a) Al_2O_3, (b) TiO_2, and (c) TiO_2/Al_2O_3 stack.

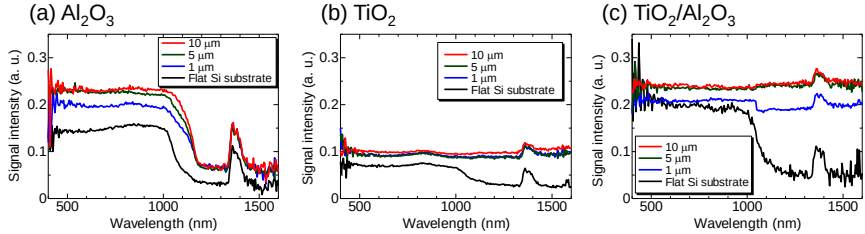

Figure 5. (a) Absorption spectra obtained by PAS.
(a) Al_2O_3, (b) TiO_2, and (c) TiO_2/Al_2O_3 stack.

The μ-PCD measurement revealed that the effective minority carrier lifetime of SiNW arrays embedded in the TiO_2/Al_2O_3 stack layer was improved from 6 to 94 μsec by the deposition of the passivation layer and post-annealing. It is noted that the effective minority carrier lifetime in TiO_2/Al_2O_3 coated SiNWs was almost the same as the Al_2O_3 coated SiNWs. It has been reported that since the fine interface between a SiNW and Al_2O_3 was formed and dangling bonds on the surface were modified by hydrogen and oxygen, the minority carrier lifetime in the SiNW arrays was improved [23]. Therefore, the improvement was achieved mainly by the passivation effect of Al_2O_3. If the stack layer was applied to the passivation films for SiNW arrays, not only the passivation

effect but also lower reflectance could be obtained. It is expected to improve the conversion efficiency of heterojunction SiNW solar cells.

Figure 6(a) shows the reflectance of SiNW solar cells covered with a 600-nm-thick Al_2O_3 single layer (black solid line), covered with a 30-nm-thick Al_2O_3/100-nm-thick TiO_2/470-nm-thick Al_2O_3 stack layer with HF etching process (blue solid line), and with RIE after the deposition of theTiO_2/Al_2O_3 stack layer (red solid line). From this figure, the reflectance of the SiNW array covered with the $Al_2O_3/TiO_2/Al_2O_3$ stack layer with the HF etching process was reduced drastically below 20% compared with SiNW fully covered with Al_2O_3. This is because the refractive index in the SiNW layer was increased. Moreover, in the case of the $Al_2O_3/TiO_2/Al_2O_3$ stack layer with RIE, the reflectance was less than around 5% in all of the wavelength range. Although the deposition of a passivation layer reduces the surface roughness of the SiNW layer, the RIE process can not only expose the top of SiNWs but also enhance the surface roughness. SiNW arrays fabricated by MACES have a tendency to form bundles after the wet etching process because of the surface tension during drying [17]. From the SEM images, the lateral size of one bundle of SiNWs with the length of 10 μm was about 1–3 μm. This causes Mie-related scattering of light in the wavelength range of visible and infrared light and the optical path length will be increased [31]. Definitely, these results suggest that the usage of the TiO_2/Al_2O_3 stack layer and RIE process can reduce the surface reflectance of heterojunction SiNW solar cells drastically.

Finally, *J-V* characteristics were measured as shown in Fig. 6(b). Red and blue lines show SiNW solar cells with the HF etching and with the RIE after the deposition of the TiO_2/Al_2O_3 stack layer, respectively. In the case of dark *J-V* characteristics, a typical rectifying property was successfully obtained for both solar cells, although leakage current can be seen. Compared with two solar cells, better characteristics were obtained in the case of the HF etching. In the case of the RIE, unintentional plasma damage was introduced on the surface of the sample. As a result, minority carrier recombination at the pn interface was increased, leading to the degradation of open-circuit voltage (V_{oc}). Moreover, the insufficient etching of the $Al_2O_3/TiO_2/Al_2O_3$ stack layer increased the series resistance (R_s) to $1.14\times10^3\ \Omega$, resulting in a decrease of the fill factor (*FF*). On the other hand, in the case with the HF etching, V_{oc}=356 mV, J_{sc}=2.96 mA/cm^2, *FF*=0.430, and E_{ff}=0.453% were obtained as shown in Table II. The reason why J_{sc} did not improve remarkably is that the TiO_2/Al_2O_3 stack layer on the top of SiNW was not removed perfectly. Therefore, a high R_s of $3.51\times10^2\ \Omega$ was still observed. It is very important to look for a way to remove the TiO_2 effectively on the top of SiNW arrays. If this issue is resolved, it is expected to improve the conversion efficiency of heterojunction SiNW solar cells due to lower reflectance.

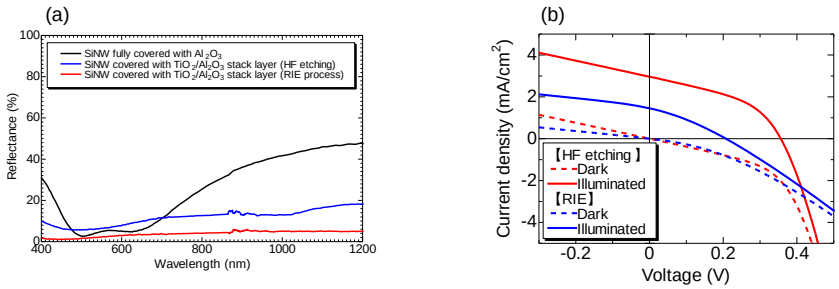

Figure 6. (a) Reflectance of SiNW solar cell covered with a 600-nm-thick Al_2O_3 single layer (black solid line), covered with a 30-nm-thick Al_2O_3/100-nm-thick TiO_2/470-nm-thick Al_2O_3 stack layer with an HF etching process (blue solid line), and with RIE (red solid line) after the deposition of theTiO_2/Al_2O_3 stack layer. (b) *J-V* characteristics of SiNW

solar cells. Red and blue lines show SiNW solar cells with HF etching and with RIE after the deposition of theTiO_2/Al_2O_3 stack layer, respectively. Dashed and solid lines show dark and illuminated *J-V* characteristics, respectively.

Table II. Solar cell parameters obtained from the illuminated *J-V* characteristics.

Etching method	V_{oc} (mV)	J_{sc} (mA/cm^2)	*FF*	R_s (Ω)	R_{sh} (Ω)	*Eff.* (%)
HF	356	2.96	0.430	3.51×10^2	2.94×10^3	0.453
RIE	207	1.45	0.308	1.14×10^3	2.95×10^3	0.093

CONCLUSIONS

To improve conversion efficiency of silicon nanowire (SiNW) solar cells, it is very important to reduce the surface recombination rate on the surface of SiNWs, since SiNWs have large surface area. To decrease surface recombination, we tried to cover SiNWs with aluminum oxide (Al_2O_3) and titanium oxide (TiO_2) by atomic layer deposition (ALD), since Al_2O_3 grown by ALD provides an excellent level of surface passivation on silicon wafers and TiO_2 has a higher refractive index than Al_2O_3, leading to a reduction of surface reflectance. The effective minority carrier lifetime in SiNW arrays embedded in a TiO_2/Al_2O_3 stack layer of 94 μsec was obtained, which was comparable to an Al_2O_3 single layer. The surface reflectance of SiNW solar cells was drastically decreased below around 5% in all the wavelength range using the $Al_2O_3/TiO_2/Al_2O_3$ stack layer. The absorptances of SiNWs with the TiO_2/Al_2O_3 stack layer were almost 100% in all the wavelength ranges from 300 to 2000 nm. Although such a parasitic absorption does not contribute to the photoelectric conversion, it is possible to realize efficient photothermal conversion devices. Heterojunction SiNW solar cells with the structure of ITO/p-type hydrogenated amorphous silicon (a-Si:H)/n-type SiNWs embedded in Al_2O_3 and TiO_2 stack layer for passivation/n-type a-Si:H/back electrode was fabricated, and a typical rectifying property and open-circuit voltage of 356 mV was successfully obtained. It is possible to improve the efficiency further by optimizing the conditions for the removal of the passivation thin films at the interface between a pn junction.

ACKNOWLEDGMENTS

This work was supported in part by Japan Science and Technology Agency (JST), PRESTO.

REFERENCES

1. L. Tsakalakos, J. Balch, J. Fronheiser, B. A. Korevaar, O. Sulima, and J. Rand, Appl. Phys. Lett. 91, 233117 (2007).
2. H. Fang, X. Li, S. Song, Y. Xu, and J. Zhu, Nanotechnology 19, 255703 (2008).
3. O. Gunawan and S. Guha, Sol. Energy Mater Sol. Cells 93, 1388 (2009).
4. V. Sivakov, G. Andrä, A. Gawlik, A. Berger, J. Plentz, F. Falk, and S. H. Christiansen, Nano Lett. 9, 1549 (2009).

5. P. Krogstrup, H. I. Jorgensen, M. Heiss, O. Demichel, J. V. Holm, M. Aagesen, J. Nygard, and A. Fontcuberta i Morral, Nat. Photon 7, 306 (2013).
6. F. Priolo, T. Gregorkiewicz, M. Galli, and T. F. Krauss, Nat. Nano 9, 19 (2014).
7. D. Kanematsu, S. Yata, A. Terakawa, M. Tanaka, and M. Konagai, Jpn. J. Appl. Phys. 54, 08KA09 (2015).
8. B. M. Kayes, H. A. Atwater, and N. S. Lewis, J. Appl. Phys. 97, 114302 (2005).
9. K. Peng, X. Wang, and S.-T. Lee, Appl. Phys. Lett. 92, 163103 (2008).
10. J. Cho, B. O'Donnell, L. Yu, K.-H. Kim, I. Ngo, and P. R. i. Cabarrocas, Prog. Photovoltaics 21, 77 (2013).
11. M. Jeon and K. Kamisako, Mater. Lett. 63, 777 (2009).
12. Y. Jiang, R. Qin, M. Li, G. Wang, H. Ma, and F. Chang, Materials Science in Semiconductor Processing 17, 81 (2014).
13. M.-D. Ko, T. Rim, K. Kim, M. Meyyappan, and C.-K. Baek, Sci. Rep. 5, 11646 (2015).
14. L. Hu and G. Chen, Nano Lett. 7, 3249 (2007).
15. C. Lin and M. L. Povinelli, Opt. Express 17, 19371 (2009).
16. S.-K. Kim, R. W. Day, J. F. Cahoon, T. J. Kempa, K.-D. Song, H.-G. Park, and C. M. Lieber, Nano Lett. 12, 4971 (2012).
17. S. Kato, Y. Watanabe, Y. Kurokawa, A. Yamada, Y. Ohta, Y. Niwa, and M. Hirota, Nanoscale Res. Lett. 8, 216 (2013).
18. R. Ishikawa, S. Kato, T. Yamazaki, Y. Kurokawa, S. Miyajima, and M. Konagai, Jpn. J. Appl. Phys. 53, 02BE09 (2014).
19. H. Savin, P. Repo, G. von Gastrow, P. Ortega, E. Calle, M. Garín, and R. Alcubilla, Nat. Nano 10, 624 (2015).
20. Y. Li, M. Li, P. Fu, R. Li, D. Song, C. Shen, and Y. Zhao, Sci. Rep. 5, 11532 (2015).
21. E. Garnett and P. Yang, Nano Lett. 10, 1082 (2010).
22. J. Zhu, Z. Yu, G. F. Burkhard, C.-M. Hsu, S. T. Connor, Y. Xu, Q. Wang, M. McGehee, S. Fan, and Y. Cui, Nano Lett. 9, 279 (2008).
23. S. Kato, Y. Kurokawa, S. Miyajima, Y. Watanabe, A. Yamada, Y. Ohta, Y. Niwa, and M. Hirota, Nanoscale Res. Lett. 8, 361 (2013).
24. S. Kato, T. Yamazaki, Y. Kurokawa, S. Miyajima, and M. Konagai, Nanoscale Res. Lett. 12, 242 (2017).
25. Y. Kurokawa, M. Yano, S. Miyajima, and A. Yamada, Jpn. J. Appl. Phys. 56, 04CS03 (2017).
26. Y. Yamada, Y. Kurokawa, S. Kato, and A. Yamada, Tech. Dig. the 23rd International Photovoltaic Science and Engineering Conference, (Taiwan, 2013) p. 1249.
27. S. Kato, Y. Watanabe, Y. Kurokawa, A. Yamada, Y. Ohta, Y. Niwa, and M. Hirota, Jpn. J. Appl. Phys. 51, 02BP09 (2012).
28. X. Li and P. W. Bohn, Appl. Phys. Lett. 77, 2572 (2000).
29. X. Chen, L. Liu, P. Y. Yu, and S. S. Mao, Science 331, 746 (2011).
30. R. Komatsu, A. Balčytis, G. Seniutinas, T. Yamamura, Y. Nishijima, and S. Juodkazis, Sol. Energy Mater Sol. Cells 143, 72 (2015).
31. G. Mie, Annalen der Physik 330, 377 (1908).